Two-photon excitation of the $4f^1 \rightarrow 5d^1$ transitions of Ce^{3+} in $LuPO_4$ and YPO_4

J. Sytsma,* D. Piehler, and N. M. Edelstein
Chemical Sciences Division, Lawrence Berkeley, Laboratory, Berkeley, California 94720

L. A. Boatner and M. M. Abraham
Solid State Division, Oak Ridge National Laboratory, Oak Ridge, Tennessee 37831
(Received 1 February 1993)

Two-photon excitation (TPE) spectra of the $4f^1 \rightarrow 5d^1$ transitions of Ce^{3+} in $LuPO_4$ and YPO_4 have been investigated. For Ce^{3+} in $LuPO_4$, transitions to four out of the five $5d^1$ levels are observed as zero-phonon lines. The symmetry properties of the levels were obtained from the polarization dependence of the TPE signals. Measurements on Ce^{3+} in YPO_4 support the given assignments. Although a crystal-field fit yields a satisfactory rms energy deviation, an unrealistic value of the spin-orbit coupling parameter, ζ_{5d^1}, is obtained. The vibronic coupling appears to be smaller than for the single-photon absorption spectra, and the vibronic bands show a rich structure. There are striking differences between the energies and the relative intensities of the vibronic lines and the associated zero-phonon lines. The vibronic coupling is also found to be strongly dependent on the Ce^{3+} concentration.

I. INTRODUCTION

The past decade has witnessed an increasing interest in the two-photon spectroscopy of lanthanide ions. This type of spectroscopy can be divided in two groups: i.e., (a) two-photon excitation (TPE), in which two photons are absorbed simultaneously by the lanthanide ion, and (b) electronic Raman scattering (ERS), in which a photon is inelastically scattered from an ion such that the ion is excited to a different electronic state. Both processes are parity allowed for the $4f \rightarrow 4f$ transitions and are to be considered as complementary to single-photon spectroscopy.

ERS is especially suited to the study of low-lying energy levels. Koningstein and Mortensen[1] and Becker *et al.*[2–4] have published ERS measurements for many lanthanide ions, and Williams *et al.*[5,6] and Piehler and Edelstein[7] have previously reported ERS for Ce^{3+} in $LuPO_4$. One practical stimulus to the study of Ce^{3+} in orthophosphates hosts is their very promising scintillator characteristics,[8] plus their potential as nuclear waste storage hosts[9] and as a tunable UV laser material.[10] The $4f^1$ crystal-field components of Ce^{3+} have energies up to $\approx 2500\ cm^{-1}$. The positions of all seven crystal-field components were determined previously[5] and resonance-enhancement effects were studied.[5–7] Calculations of these effects rely heavily on the positions and symmetry assignments of the $5d^1$ levels.[11] Despite a large amount of single-photon spectroscopic data for Ce^{3+} in the orthophosphates, only the first $5d^1$ level has been determined accurately. Our goal was to apply TPE to Ce^{3+} in $LuPO_4$ in order to obtain this information for the other $5d^1$ levels as well. Measurements were also performed for Ce^{3+} in YPO_4 in order to confirm the $LuPO_4$ results.

Although TPE was discovered in 1962,[12] the work by Downer *et al.*[13] reawakened interest in TPE for the lanthanides.[14] Downer *et al.* showed that the original theory proposed by Axe[15] does not provide satisfactory agreement with the experimental data for the ions Gd^{3+} and Eu^{2+}. Selection rules were violated, the polarization anisotropy was not predicted correctly, and the experimental intensities were anomalously large. The inclusion of higher-order terms in the calculations has been shown[16,17] to overcome these discrepancies. Judd and Pooler[18] have suggested that the deviation from Axe's theory will be most pronounced for Gd^{3+} and Eu^{2+} because of their half-filled f shell. Axe's theory, however, does not work well for the case of Pr^{3+} either.[19] Calculations for Pr^{3+} have unfortunately not been published based on the theory of Downer *et al.* at the present time, and so a comparison is not possible for this case.

Ce^{3+} has a unique position among the lanthanide ions since the total $4f$ splitting is $\approx 2500\ cm^{-1}$. Therefore, for Ce^{3+} ERS will be the only practical parity-allowed two-photon spectroscopy technique. The next-highest levels are from the $5d^1$ configuration and typically start at $30\,000\ cm^{-1}$. In principle, TPE to these levels is parity forbidden. For Ce^{3+} at a noncentrosymmetric site, however, odd crystal-field components will mix opposite-parity configurations with the $5d$ configuration. Interactions with odd-parity phonons will result in a similar configuration mixing. This makes the $4f \rightarrow 5d$ TPE transitions forced-electric-dipole allowed. These are essentially the same mechanisms that make $4f \rightarrow 4f$ single-photon forced-electric-dipole transitions allowed.

In earlier work using TPE for the case of Ce^{3+}, the Ce^{3+} ion occupied several sites in the host lattices. This significantly hampered an accurate assignment, espe-

cially for the symmetries of the components. Gayen, Hamilton, and Bartram reported on the TPE of Ce^{3+} in CaF_2.[20,21] They observed the zero-phonon transition from the $4f^1(^2F_{5/2})$ ground state to the first component of the $5d^1$ configuration and measured the absolute cross section $\sigma(\theta = 0°) = 2 \times 10^{-54}\,\mathrm{cm}^4\,\mathrm{s}$, with an estimated factor of 5 uncertainty. Calculations of the cross section turn out to give much larger values.[21] Leavitt has elaborated on the static and dynamic contributions to the lowest $4f \rightarrow 5d$ TPE transition and found better agreement.[22] Using a different approach, Makhanek, Karolkov, and Yuguryau also found good agreement.[23]

The Ce^{3+} ions do not have a unique site symmetry in Ce^{3+}:CaF_2 because of the charge compensation which is necessary for the trivalent cerium ion substituting for the divalent calcium ion. Instead, there are several Ce^{3+} sites, each with slightly different energy splittings. Consequently, the inhomogeneous broadening is considerable.[20,24,25] Pedrini *et al.*[26] used TPE to study Ce^{3+} in LaF_3. The resolution they show, however, is not sufficient to determine zero-phonon line positions; moreover, they conclude that for larger concentrations several sites and numerous traps are present.

All of the experimental studies[20,24–26] show that vibronic effects play an important role in the TPE of Ce^{3+}. A major part of the intensity arises from TPE transitions to a final state in which the electronic state is coupled to a vibrational state. For Ce^{3+} in CaF_2, the vibronic contribution in the TPE transitions to higher $5d^1$ levels is so large that the zero-phonon lines are unobservable.[24,25] In addition, the vibronic bands tend to be structureless; i.e., transitions to different vibrational states do not show up as distinctive peaks. This is also the case for Ce^{3+} in $LiYF_4$.[27]

For the TPE of Ce^{3+} in $LuPO_4$, transitions to four out of the five $5d^1$ levels are observed as zero-phonon lines. The positions of these levels have been measured directly. (The wavelengths necessary for TPE to the fifth component were not attainable with our equipment.) The vibronic coupling is small, and the vibronic bands show a rich structure. The respective symmetry labels for the $5d^1$ levels were obtained from the polarization dependence of the TPE signal. The derived symmetry labels are supported by TPE data obtained for the isostructural YPO_4 host.

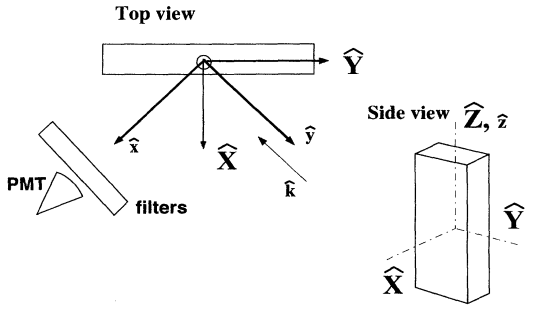

FIG. 1. Schematic diagram of the crystal-symmetry axes ($\hat{\mathbf{X}}$, $\hat{\mathbf{Y}}$, and $\hat{\mathbf{Z}}$) and the local symmetry axes for the Ce^{3+} ion ($\hat{\mathbf{x}}$, $\hat{\mathbf{y}}$, and $\hat{\mathbf{z}}$). In the top view drawing, $\hat{\mathbf{Z}}$ and $\hat{\mathbf{z}}$ are perpendicular to the surface of the figure, coming out of the paper. Incident excitation light is parallel to $\hat{\mathbf{y}}$ ($\hat{\mathbf{k}} \parallel \hat{\mathbf{y}}$); induced luminescence is viewed along $\hat{\mathbf{x}}$.

II. SAMPLE PREPARATION AND PROPERTIES

A. Orthophosphates $LuPO_4$ and YPO_4

Single crystals of $LuPO_4$ and YPO_4 were grown using a flux method described previously.[28] Typical sample dimensions were 0.5 mm × 4 mm × 10 mm. Only crystals exhibiting good optical quality were selected.

The host lattices $LuPO_4$ and YPO_4 both have the tetragonal zircon-type structure with space group D_{4h}^{19}. We write the reference axes for the space-group symmetry as $\hat{\mathbf{X}}$, $\hat{\mathbf{Y}}$, and $\hat{\mathbf{Z}}$. $\hat{\mathbf{Z}}$ is the optical axis of the crystal, while $\hat{\mathbf{X}}$ and $\hat{\mathbf{Y}}$ are two equivalent axes. The site symmetry for the rare-earth ions is D_{2d}. The Ce^{3+} ion substitutes for the Lu^{3+} or Y^{3+} ion. The reference axes for the D_{2d} operations, which we write as $\hat{\mathbf{x}}$, $\hat{\mathbf{y}}$, and $\hat{\mathbf{z}}$, are different from the axes for the crystal-symmetry operations. The $\hat{\mathbf{x}}$ and $\hat{\mathbf{y}}$ axes are obtained by a rotation of $\pi/4$ about the $\hat{\mathbf{Z}}$ axes (see Fig. 1). The crystals are birefringent with indices of refraction $n_0 = 1.694$ and $n_e = 1.728$ for $LuPO_4$ (Ref. 29) and $n_0 = 1.721$ and $n_e = 1.816$ for YPO_4 (Ref. 30) at $\lambda = 589.3$ nm.

Rare-earth orthophosphates crystallize in two different crystal structures. For the smaller rare-earth ions (Tb^{3+} to Lu^{3+}), the structure is that of YPO_4 (xenotime), the tetragonal zircon structure. For the larger rare-earth ions (Ce^{3+} to Gd^{3+}), the structure is monoclinic (monazite).[31] This difference in crystal structure will limit the amount of Ce^{3+} that can be doped into $LuPO_4$ and YPO_4 without changing the crystal structure. We have used crystals with, at most, 8 mol % of cerium relative to lutetium in the starting materials. X-ray fluorescence and mass spectrometric analyses show that the actual Ce^{3+} concentration in the crystals is much smaller, approximately 2% of the starting material concentration.[6,8]

B. $5d^1$ configuration of Ce^{3+} in orthophosphates

The $5d^1$ configuration of Ce^{3+} in D_{2d} symmetry is split into four components by the crystal field. Inclusion of the spin-orbit coupling gives an additional splitting for one of the components, but this splitting will be small compared to the crystal-field splitting. Figure 2 shows the splittings of the $5d^1$ configuration with labels of the irreducible representation of the D_{2d} group and inclusion

TABLE I. Observed $5d^1$ crystal-field components for Ce^{3+} in YPO_4.

Reference 34 E (cm^{-1})	Reference 35 E (cm^{-1})	Reference 38 E (cm^{-1})
32 800	30 769	31 192
36 900	39 683	40 262
	41 841	42 360
41 500	44 529	46 714
	49 261	

of the spin-orbit coupling.

Single-photon spectroscopy of Ce^{3+} in $LuPO_4$ has been reported previously by Hoshina and Kuboniwa,[32] Nakazawa and Shionoya,[33] Williams *et al.*,[5] and Piehler and Edelstein.[7] These papers report, for the most part, either in absorption or in emission, transitions between the $4f^1$ levels ($^2F_{5/2}$ and $^2F_{7/2}$) and the lowest component of the $5d^1$ configuration. Williams *et al.*[5] did experiments in which the positions of all the components of both the $4f^1$ and the $5d^1$ configurations were determined. Symmetry assignments were based on electronic-Raman-scattering selection rules for the $4f^1$ configuration and on a crystal-field fit for the $5d^1$ configuration. Earlier work on Ce^{3+} in YPO_4, giving only the energy positions of the $5d^1$ configuration, was reported by Blasse and Bril[34] and Ropp.[35] In later investigations, symmetries were assigned by Briffault and Denis[36] and Balasubramian and Newman.[37] Both of these latter reports neglected spin-orbit coupling and did not use the double-group representation to label the symmetries. Additionally, Karanjikar and Naik[38] have reported x-ray-excited luminescence and excitation spectra of powders of 1% Ce^{3+} in YPO_4.

In all of these previous studies, the only allowed, directly observed zero-phonon line was from the $4f^1(^2F_J) \rightarrow 5d_1^1(J = 5/2, 7/2)$ transition, $5d_i^1$ denoting the ith $5d^1$ component. Note that Ref. 32 reports five zero-phonon lines, but in fact several vibronic lines were incorrectly assigned as zero-phonon lines. Positions of the higher-lying $5d^1$ components were estimated either from the origin and width of vibronic bands or from crystal-field fits. All of this work is summarized in Tables I and II.

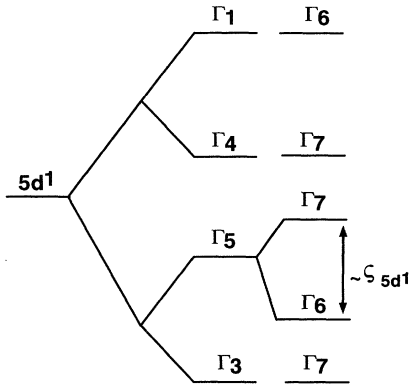

FIG. 2. Schematic energy diagram for Ce^{3+} in a D_{2d} symmetry. Energy levels are not to scale. The symmetry assignments are derived in this work.

III. EXPERIMENTAL DETAILS

A. Experimental instrumentation

All measurements described here were performed at liquid-helium temperature. We used an Oxford CF 1204 optical cryostat to cool the samples to ~ 4.2 K.

Single-photon, high-resolution measurements were made using a 60-W D_2 lamp with the light focused on the sample by a lens with $f = 7.5$ cm. The transmitted light was collected by an $f = 20$ cm lens, focused on the entrance slits of a Spex 1403 double monochromator, and was detected with a cooled Hamamatsu 943-02 photomultiplier tube (PMT). Typically, the slit widths were 200 μm, which resulted in a resolution of ≤ 2 cm^{-1}. Since the monochromator does not operate above 30 500 cm^{-1}, it was used in second order. A Corning 7-54 filter was used to stop the visible part of the lamp spectrum.

The core of the experimental instrumentation for the TPE is a PDL-1 dye laser pumped by a DCR-1A Nd-YAG laser, both from Quanta Ray. This system gives tunable, vertically polarized light. To cover the region from 615 nm to 675 nm, we used the second harmonic of the Nd-YAG laser to pump a solution of DCM dissolved

TABLE II. Observed $5d^1$ crystal-field components and their symmetry assignments for Ce^{3+} in YPO_4 (Ref. 36) and $LuPO_4$ (Ref. 5), using the irreducible representation of the D_{2d} group and with inclusion of the spin-orbit coupling. Labels in parenthesis are valid if the spin is neglected.

Reference 36		Reference 37		Reference 5	
E (cm^{-1})	Symmetry	E (cm^{-1})	Symmetry	E (cm^{-1})	Symmetry
		21 233 [a]	$\Gamma_7(\Gamma_4)$		
30 970	$\Gamma_6 \oplus \Gamma_7(\Gamma_5)$	30 970 [b]	$\Gamma_6 \oplus \Gamma_7(\Gamma_5)$	30 468	Γ_7
35 870	$\Gamma_7(\Gamma_3)$	35 870 [b]	$\Gamma_6(\Gamma_1)$		
39 514	$\Gamma_7(\Gamma_4)$	39 514 [b]	$\Gamma_7(\Gamma_3)$	39 931	Γ_6
				41 626	Γ_7
				44 038	Γ_6
50 000	$\Gamma_6(\Gamma_1)$			50 290	Γ_7

[a]Calculated using modelled values for the crystal field.
[b]Energy values from Ref. 36.

in methanol. For the region from 445 to 525 nm, we used the dyes Coumarin 460 and LD 489 in methanol and the third harmonic of the Nd-YAG laser as a pump beam. The scanning of the dye laser was controlled by a program running on an AT microcomputer.

The polarization of the excitation light was controlled with a Soleil Babinet Compensator (SB-10) from Optics for Research. The beam passed a 10% reflector and was focused on the sample with an aplanant lens ($f = 15$ cm). Light from the reflector was detected by an EG&G SGD-100A photodiode for normalization purposes. TPE was detected by monitoring the overall Ce^{3+} emission. This luminescence was detected by a Hamamatsu 928 PMT located at an angle of 90° to the laser beam (see Fig. 3).

The polarization vector $\hat{\epsilon}$ has to be given with respect to the local symmetry axes, i.e., with respect to $\hat{x}$, $\hat{y}$, and $\hat{z}$. The sample was placed in the cryostat such that the laser beam hit the sample surface at an angle ϕ_0 of 45°. This implies that, at the surface of the sample, $\hat{k} \parallel \hat{y}$, with $\hat{k}$ the wave vector of the excitation light (see Fig. 1). The angle of refraction will then be $\approx 25°$. The PMT was covered with the appropriate filter to reduce detection of direct scattered laser light.

For each laser pulse, the signals from the PMT and the photodiode were sent to SR 250 boxcar integrators (Stanford Research Systems). The boxcars were triggered by a pulse from a second photodiode, monitoring a residue of the second harmonic of the Nd-YAG laser. To discriminate the luminescence further from direct reflected laser light, we used a delay of 10 ns on the boxcar integrating the PMT signal. A gate width of 30 ns was used, since the lifetime of the main luminescence is 20 ns (Ref. 10) (see Fig. 3).

Single-shot intensities from both boxcars were directed to an SR 245 computer interface and read by the AT microcomputer. The luminescence intensity was normalized versus the square of the laser intensity. For each point in a spectrum, typically 60 shots were averaged. Both the normalized intensity and the laser intensity were stored as a function of the wavelength. This permitted checks on the whether the spectral features were "real" or were induced by transients in the laser intensity during the normalization procedure. Polarization dependency curves were corrected for the polarization dependence of the normalization reflection.

B. Results

TPE spectra were measured for different concentrations of Ce^{3+}. Within the experimental accuracy, $\pm 1\,cm^{-1}$, we do not observe a change in the positions of the transitions. (The positions are given in vacuum wave numbers.)

Figure 4 shows the two-photon excitation spectrum of Ce^{3+} in $LuPO_4$ which consists of a sharp zero-phonon line at 15 227.8 cm^{-1} ($= 1/2 \times 30\,455.6\,cm^{-1}$) and a large number of vibronic lines extending to 15 950 cm^{-1} ($= 1/2 \cdot 31\,900\,cm^{-1}$). In the same figure, a high-resolution single-photon absorption spectrum is shown for comparison. This absorption spectrum is essentially the same as the one shown in Refs. 5 and 7. From the comparison with the single-photon absorption spectrum, we attribute the line at 15 227.8 cm^{-1} to TPE to the lowest component of the $5d^1$ configuration. Vibrational modes with energies up to 1500 cm^{-1} are involved in the two-photon transition. Surprisingly, the ratio of vibronic intensity to zero-phonon intensity, r, is largest for the single-photon absorption spectrum. Since TPE is only possible through parity mixing by odd crystal-field terms and odd-parity vibrational modes, one might expect this to be reversed. Figure 5 shows a drastic increase in vibronic intensity, for increasing Ce^{3+} concentration.

The polarization has two degrees of freedom: ϕ, the

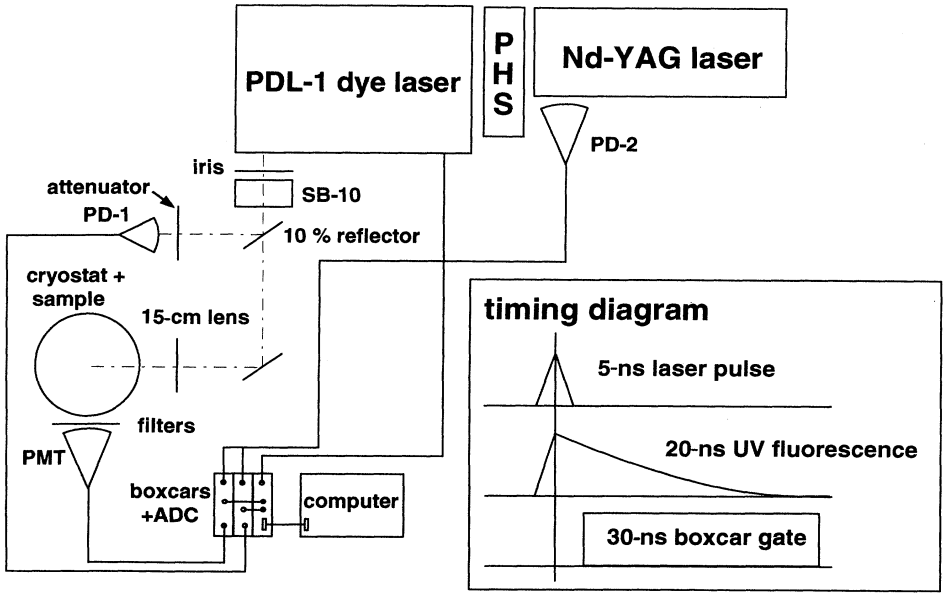

FIG. 3. Experimental system. The PHS is a prism harmonic separator to select the appropriate pump beam. PD-1 is the normalization photodiode; PD-2 is the photodiode giving the trigger pulse to the boxcar integrators. Intensities of both boxcars are read via the analog digital convertor (ADC) of the SR 245 computer interface. The timing diagram is for the boxcar measuring the TPE luminescence.

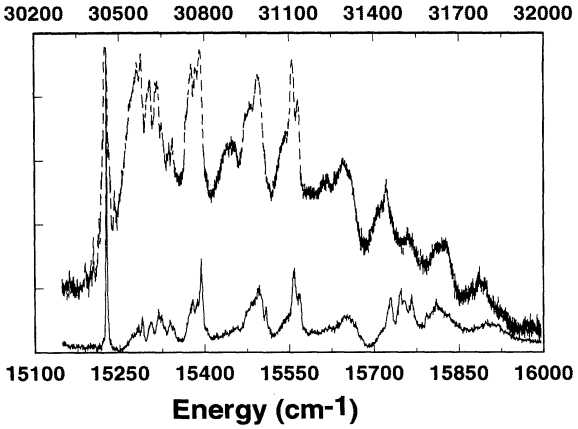

FIG. 4. Two-photon excitation spectrum of Ce^{3+} in $LuPO_4$ (solid line, lower axis) to the first of the $5d^1$ components. The polarization of the excitation light was parallel to the $\hat{\mathbf{z}}$ axis. The dashed line (upper axis) is a (unpolarized) single-photon absorption spectrum of the same crystal. Both spectra are measured at 4.2 K.

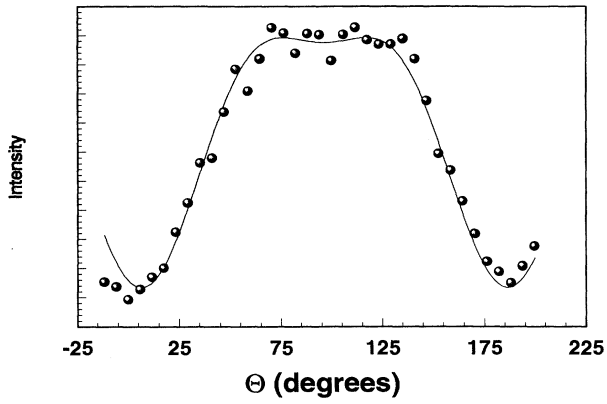

FIG. 6. TPE signal as a function of the polar angle θ of the polarization vector $\hat{\epsilon}$. Excitation is at 15 227.8 cm^{-1}.

angle of $\hat{\epsilon}$ with respect to the $\hat{\mathbf{x}}$ axis, and θ, the angle of $\hat{\epsilon}$ with respect to the $\hat{\mathbf{z}}$ axis. Since the crystals are so thin (typically 0.5 mm), we were only able to measure the θ dependence of the TPE luminescence intensity. For the zero-phonon line at 15 227.8 cm^{-1} the result is shown in Fig. 6.

According to Williams *et al.*,[5] the $5d_2^1$ and $5d_3^1$ components are expected to be at 39 931 and 41 626 cm^{-1}, respectively. TPE to these components is thus expected around 19 415 and 20 811 cm^{-1}, respectively. Instead, we observe two lines near 19 847 cm^{-1} ($= 1/2 \cdot 39\,694\,cm^{-1}$) separated only by 4.5 cm^{-1} (Fig. 7). The polarization dependence and the coupling to lattice vibrations of the two lines are strikingly different. No additional zero-phonon lines are observed up to 21 050 cm^{-1} ($= 1/2 \cdot 42\,100\,cm^{-1}$). Changing the delay and gate widths of the boxcar integrator do not change the relative intensities of the two lines, nor do changes of the filter in front of the PMT. The spectral and temporal characteristics of the TPE luminescence are thus the same for both excitation transitions.

TPE was also measured for Ce^{3+} in the isostructural host YPO_4 in the region of 19 000–20 000 cm^{-1}. Again, two zero-phonon lines were detected at only slightly different positions than for Ce^{3+} in $LuPO_4$. The polarization-dependency curves show a similar behavior as for Ce^{3+} in $LuPO_4$. The coupling to lattice vibrations differs strongly for these two lines, similar to what was observed for Ce^{3+} in $LuPO_4$ (see Fig. 8). A fourth line

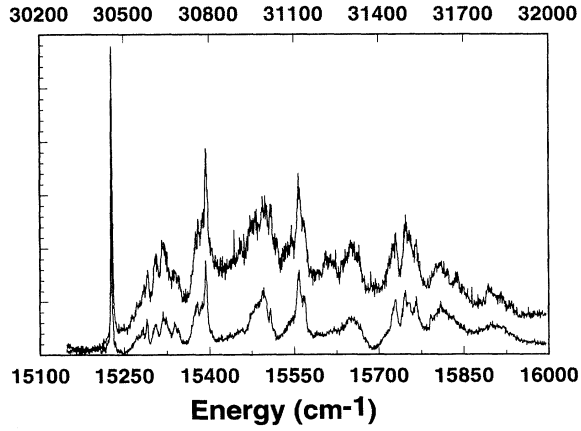

FIG. 5. Two-photon excitation spectrum of Ce^{3+} in $LuPO_4$ to the first of the $5d^1$ components, for two different concentrations of Ce^{3+}. The upper curve is for a relative starting-material concentration of 2%, the lower curve for 0.8%. The spectra are scaled such that the zero-phonon lines have equal peak intensity.

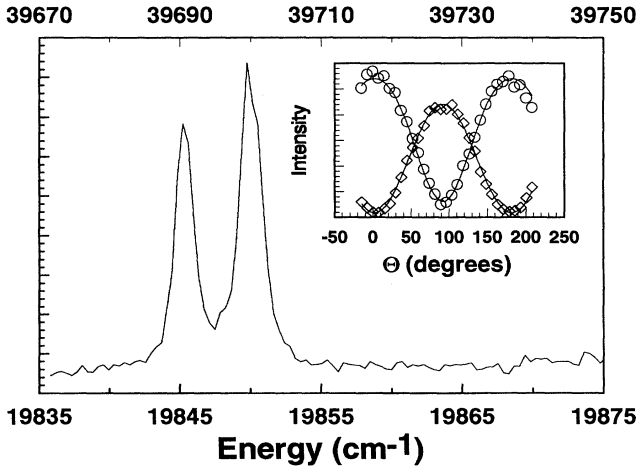

FIG. 7. Two-photon excitation spectrum of Ce^{3+} in $LuPO_4$ to the second and third $5d^1$ components for different polarizations of the excitation light. The inset shows the TPE signal as a function of the polar angle θ of the polarization vector $\hat{\epsilon}$. Excitation is at 19 845.3 cm^{-1} (○) and at 19 849.8 cm^{-1} (◇).

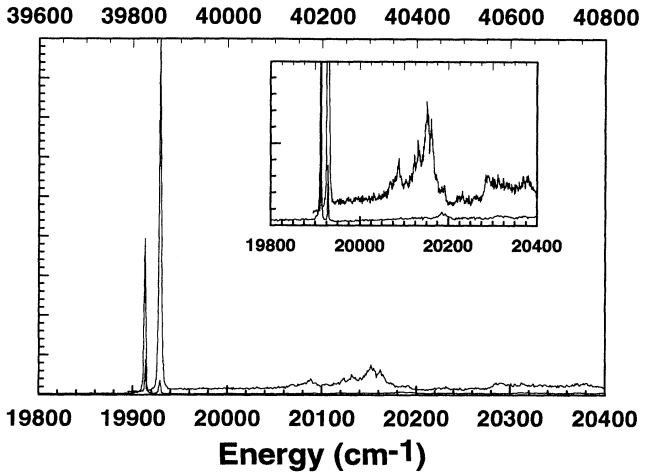

FIG. 8. Differences in vibronic coupling for TPE transitions of Ce^{3+} in YPO_4 (solid line $\theta = 90°$, dashed line $\theta = 0°$). Because of polarization leakage, the zero-phonon line at 19 929.0 cm^{-1} shows up in the dashed spectrum as well.

was observed at 22 196.5 cm^{-1} ($= 1/2 \cdot 44\,393\,cm^{-1}$), as is shown in Fig. 9. This is, again, in good agreement with the data from Ref. 5. The intensity is considerably weaker than the intensities of the other lines. The polarization dependence of this line is shown in Fig. 9 as well.

The positions of the observed zero-phonon lines are summarized in Table III. The fifth $5d^1$ component is expected at about 50 000 cm^{-1}. For TPE this requires tunability around 400 nm, whereas the lowest possible wavelength from the PDL-1 is $\approx$ 440 nm.

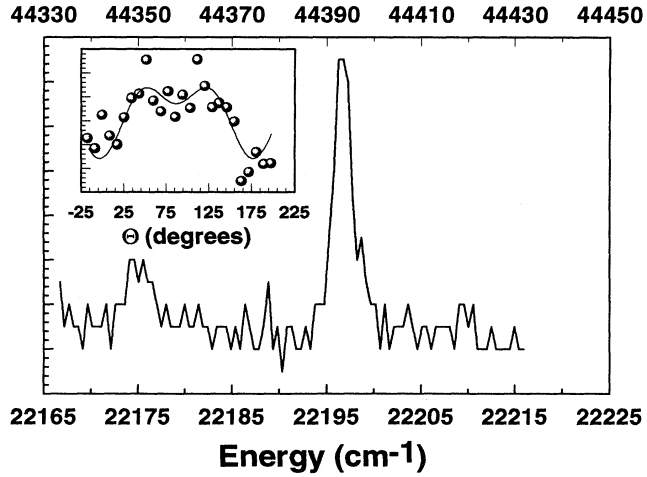

FIG. 9. Two-photon excitation spectrum of Ce^{3+} in $LuPO_4$ to the fourth of the $5d^1$ components. The polarization of the excitation light was parallel to the $\hat{z}$ axis. The inset shows the TPE signal as a function of the polar angle θ of the polarization vector $\hat{\epsilon}$. Excitation is at 22 196.5 cm^{-1}.

TABLE III. Positions and symmetries of the first four crystal-field components of the $5d^1$ configuration of Ce^{3+} in $LuPO_4$.

E (cm^{-1})				
$LuPO_4$		YPO_4		
Zero-phonon line	$5d_i^1$	Zero-phonon line	$5d_i^1$	Symmetry
15 227.8	30 455.6			Γ_7
19 845.3	39 690.6	19 913.0	39 826.0	Γ_6
19 849.8	39 699.6	19 929.0	39 858.0	Γ_7
22 196.5	44 393.0			Γ_7

IV. DISCUSSION

A. Theoretical considerations

1. Polarization dependence

The site symmetry of the Ce^{3+} ion imposes selection rules on the TPE transitions. From these rules one can deduce the symmetry of the $5d^1$ components. Qualitative group-theory analysis shows that the selection rules for D_{2d} symmetry are

$$\Gamma_6 \rightarrow \Gamma_6 \text{ allowed for } \hat{\epsilon} \parallel \hat{x}, \hat{y}, \hat{z},$$
$$\Gamma_6 \rightarrow \Gamma_7 \text{ allowed for } \hat{\epsilon} \parallel \hat{x}, \hat{y}.$$

The $4f^1$ ground state has Γ_6 symmetry, and the $5d^1$ components have either Γ_6 or Γ_7 symmetry.

A more quantitative analysis[39–41] gave the dependence of the TPE luminescence intensity $S_{\Gamma_i \rightarrow \Gamma_f}$ on the polar angles of $\hat{\epsilon}$. For a $\Gamma_6 \rightarrow \Gamma_7$ transition, this dependence is given by[39]

$$S_{\Gamma_6 \rightarrow \Gamma_7} = \sin^4(\theta)\cos^2(2\phi) + c_1 \sin^4(\theta)\sin^2(2\phi) + c_2 \sin^2(2\theta). \quad (1)$$

Here, ϕ and θ are the polar angles of $\hat{\epsilon}$ with respect to the $\hat{x}$ and $\hat{z}$ axes. Daoud and Kibler[41] have given explicit expressions for the coefficients, but we will use them as empirical parameters since in this case it is not necessary to know the absolute intensities of the TPE transitions. Since the crystals are relatively thin, we were only able to vary θ. The dependence on ϕ is taken as an empirical parameter, since ϕ is constant. Equation (1) then simplifies to

$$S_{\Gamma_6 \rightarrow \Gamma_7} = c_1' \sin^4(\theta) + c_2 \sin^2(2\theta). \quad (2)$$

For the $\Gamma_6 \rightarrow \Gamma_6$ transition the relation is[39]

$$S_{\Gamma_6 \rightarrow \Gamma_6} = \lambda^2 + (\lambda - 1)(\lambda - 3)\sin^2(\theta) + [c_3 - \tfrac{1}{4}(\lambda - 1)^2]\sin^2(2\theta), \quad (3)$$

which is independent of ϕ.

Under D_{2d} symmetry, the metal-ion site is uniaxial. This anisotropy is taken into account in the derivation of Eqs. (2) and (3).[40] The transmittance of light in the crystal is dependent on the direction of the polarization

with respect to the plane of incidence. The dependence is given by the well-known Fresnel coefficients

$$T_\perp = \frac{\sin(2\alpha_0)\sin(2\alpha)}{\sin^2(\alpha_0+\alpha)},$$
$$T_\parallel = \frac{T_\perp}{\cos^2(\alpha_0-\alpha)},$$

where $T_{\perp(\parallel)}$ is the transmittance for light polarized perpendicular (parallel) to the plane of incidence, α_0 is the angle of incidence, and α is the angle of refraction. In our case, the plane of incidence is the $\hat{\mathbf{x}}\hat{\mathbf{y}}$ plane, and so $T_{\perp(\parallel)}$ is the transmittance for light parallel (perpendicular) to the $\hat{\mathbf{z}}$ axis and $\alpha = \phi$. To account for the difference in transmittance we rewrite[42] Eqs. (2) and (3) as

$$S_{\Gamma_6\to\Gamma_7} = T_\parallel^2 c_1' \sin^4(\theta) + T_\perp T_\parallel c_2 \sin^2(2\theta), \quad (4)$$
$$S_{\Gamma_6\to\Gamma_6} = \lambda^2 T_\perp^2 + (\lambda T_\perp - T_\parallel)(\lambda T_\perp - 3T_\parallel)\sin^2(\theta) + [c_3 T_\perp T_\parallel - \tfrac{1}{4}(\lambda T_\perp - T_\parallel)^2]\sin^2(2\theta). \quad (5)$$

$T_\perp$ and $T_\parallel$ depend only on the angle of incidence and the index of refraction. These are constant parameters during the experiments, and thus $T_\perp$ and $T_\parallel$ are constant. With $\phi_0 = 45°$ and the index of refraction 1.7 we have $\phi = 24.5°$, $T_\perp = 0.86$, and $T_\parallel = 0.98$.

Two features of the functions given in Eqs. (4) and (5) permit a definitive symmetry assignment for the components of the $5d^1$ configuration. First, Eq. (4) becomes zero for $\theta = 0$, and thus the transition $\Gamma_6 \to \Gamma_7$ is forbidden for $\hat{\epsilon} \parallel \hat{\mathbf{z}}$. The $\Gamma_6 \to \Gamma_6$ transition is, according to Eq. (5), allowed for $\theta = 0$. This is according the qualitative selection rules given previously. Second, all of the fit parameters c_i and λ have to be real and, except for λ, positive.[39]

It is obvious from the spectra (Figs. 4 and 8) that TPE occurs to final states in which the electronic and vibrational states are coupled. The symmetries of such a state will be the direct product of the irreducible representations of the purely electronic state and the vibrational state. Thus the vibronic part of the spectrum will not have a uniform polarization behavior, and it may differ from the polarization dependence of the zero-phonon line. To assign symmetry labels to the $5d^1$ components, we have to measure the polarization dependence of only the zero-phonon lines, not somewhere in the vibronic spectrum. Therefore, the exact position of the $5d^1$ components has to be known.

2. *Crystal-field model*

The positions and symmetry assignments of the four $5d^1$ components were fitted with a semiempirical Hamiltonian. The wave functions obtained from diagonalizing this Hamiltonian can be used in calculations of absolute cross sections of the ERS transitions.[5,7] The Hamiltonian is of the form

$$\mathcal{H} = F_0 + \mathcal{H}_{\text{spin orbit}} + \mathcal{H}_{\text{crystal field}}, \quad (6)$$

where

$$\mathcal{H}_{\text{spin orbit}} = \zeta_{5d^1}(\mathbf{s}\cdot\boldsymbol{l}),$$
$$\mathcal{H}_{\text{crystal field}} = B_0^2 C_0^2 + B_0^4 C_0^4 + B_4^4 (C_4^4 + C_{-4}^4).$$

Here, F_0 fixes the average energy of the $5d^1$ configuration relative to the ground state and ζ_{5d^1} is the spin-orbit coupling parameter that determines the splitting of the Γ_5 state into Γ_6 and Γ_7 components (Fig. 2). It is expected to be close to the value of the free-ion spin-orbit coupling parameter. The B_q^k's are the crystal-field parameters and determine the overall splitting. Since we are considering a $5d$ configuration, $k \le 4$. F_0, ζ_{5d^1}, and B_q^k are treated as empirical parameters. In the fits, a fifth level was assumed at to lie 50 000 cm^{-1}.

B. Discussion of the results

From the comparison with the single-photon absorption spectrum, we already attributed the TPE line at 15 227.8 cm^{-1} to the transition of the $4f^1(^2F_{5/2})$ ground state to the first component of the $5d^1$ configuration. Williams *et al.* assigned a Γ_7 symmetry to this component on the basis of the single-photon absorption selection rules.[5] Therefore, we fitted the polarization curve for this transition (Fig. 6) to Eq. (4). This gives good results, as can be seen in Fig. 6 and confirms the earlier symmetry assignment. The fit parameters obtained from this fit are given in Table IV.

The Raman- and infrared-active lattice vibrations have energies up to 1170 cm^{-1}.[43,44] Since the vibronic sideband extends to more than 1500 cm^{-1} away from the zero-phonon line, it is clear that excitation can involve more than one vibrational mode. Polarization effects will reflect the symmetries of the zero-phonon line and of the vibrations involved. To derive the symmetries of the purely electronic states from polarization effects in the vibronic sideband, one has to know the symmetries of all vibrations involved. When there is more than one mode involved, this is a formidable task and has not been attempted.

It is much more difficult to assign the second and third $5d^1$ components. Williams *et al.*[5] locate them at 39 931 and 41 626 cm^{-1} and have assigned the symmetry labels Γ_6 and Γ_7, respectively. Their relative starting-material

TABLE IV. Final values of the parameters in the fits of the polarization dependency curves of TPE transitions in Ce^{3+} in $LuPO_4$.

Transition	Fit parameters				
E (cm^{-1})		30 455.6	39 690.6	39 699.6	44 393.0
$\Gamma_6 \to \Gamma_7$	c_2/c_1'	0.63		0.28	1.08
$\Gamma_6 \to \Gamma_6$	λ, c_3		2.6828, 0.6170		

concentration was much higher than the one used here (viz., 20% versus 1%). This large concentration difference leads to shifts in the energy positions of the $5d^1$ components, as is apparent from the position of the first component (30 468 versus 30 455 cm^{-1}; see Tables II and III). It is thus reasonable to assume that one of the lines in Fig. 7 must be attributed to the $^2F_{5/2} \rightarrow 5d_2^1$ transition, having Γ_6 polarization characteristics. The question is, which one and how does the other line arise? No previous study has reported the second and third components so close to each other as shown in Fig. 7. We observed such closely separated lines for different concentrations of Ce^{3+} in $LuPO_4$ and for Ce^{3+} in YPO_4. From the spectroscopic measurements it seems reasonable to assign these lines to the TPE transitions of $^2F_{5/2}$ to the $5d_2^1$ and $5d_3^1$ components.

Since the spectral and temporal characteristics of the TPE signals are the same for both lines, both features can be assigned to $4f^1 \rightarrow 5d^1$ transitions of the Ce^{3+} ion. Increasing the Ce^{3+} concentration results in broadening and eventually the merging of both lines. The relative intensities of both lines remains approximately the same as the Ce^{3+} concentration is lowered. The energy-level diagrams of Carnall, Crosswhite, and Crosswhite[45] show that no other rare-earth ion, the most likely impurity, has a transition in this region.

The observed small separation suggests that there are two different sites available for the Ce^{3+} ion, which is not unreasonable from the structural point of view, since $LuPO_4$ crystallizes in a different crystal structure than $CePO_4$. Even the highest-resolution measurements possible on the transitions to the first and fourth (see below) components, however, do *not* reveal two closely separated zero-phonon lines, which rules out the presence of two different sites. Moreover, the intensity ratio of the two lines is approximately the same for different Ce^{3+} concentrations.

The lowest transition of the two features, at 19 845.3 cm^{-1}, shows a distinctly different polarization dependence (Fig. 7) than the transition to the first component (Fig. 6). A fit to Eq. (5) gives a good result (Fig. 7) whereas a fit to Eq. (4) yields the unrealistic result of $c_1' < 0$. The line at 19 849.8 cm^{-1} shows a similar polarization dependence as the transition to the first $5d^1$ component and can indeed be fitted to Eq. (4). The fit parameters obtained from these fits are also given in Table IV.

Finally, we note that no other zero-phonon lines are observed up to $1/2 \times (42\,100)\,cm^{-1}$, well beyond the energy where Williams *et al.* locate the $5d_3^1$ component. Therefore we suggest that the second component of the $5d^1$ configuration is at $2 \times 19\,845.3 = 39\,690.6\,cm^{-1}$ and has Γ_6 symmetry, and the third component is at $2 \times 19\,849.8 = 39\,699.6$ cm^{-1} and has Γ_7 symmetry. We can apply similar assignments for the case of Ce^{3+} in YPO_4. We ascribe the line at 22 196.5 cm^{-1} to a TPE transition to the $5d_4^1$ component. The position for this component is in reasonable agreement with the assignment by Williams *et al.* The fit for the polarization curve in Fig. 9 is to Eq. (4) and the parameters are given in Table IV. This makes it clear that this is a $\Gamma_6 \rightarrow \Gamma_7$ transition, and thus the $5d_4^1$ component has Γ_7 symmetry. The positions and the assigned symmetry labels for the Ce^{3+} $5d^1$ components in $LuPO_4$ and YPO_4 are presented in Table III.

The crystal-field fit for Ce^{3+} in $LuPO_4$ yields a rms energy deviation of only 4.2 cm^{-1}. The final-fit parameters are given in Table V. Even though the general agreement between experimental and calculated positions is very good, Table V shows a disturbing result. The spin-orbit coupling parameter ζ_{5d^1} is much smaller than expected, the free-ion value being 995.6 cm^{-1}.[46] It can be argued that a purely electrostatic crystal-field Hamiltonian will not correctly describe covalency between the excited Ce^{3+} ion and the ligand ions. The major effect of the spin-orbit coupling, however, is to split the Γ_5 crystal-field component into a Γ_6 and a Γ_7 component. The validity of the crystal-field Hamiltonian does not consequently affect the value of ζ_{5d^1}. The spin-orbit coupling parameter has to be close to the separation between these two components. With $\zeta_{5d^1} = 9.29$ and $\Delta E_{\Gamma_6\Gamma_7} = 9.3$ we find a consistency between the data and the fit.

If we fix ζ_{5d^1} at the free-ion value, we obtain a rms deviation of approximately 340 cm^{-1}. For a d configuration, this is not an unreasonable accuracy, but, of course, in this case the spin-orbit coupling parameter is not consistent with the data. The values of the parameters for this fit are shown in Table V.

The value of the spin-orbit coupling constant ζ_{5d^1} obtained from the above fit is unreasonable. Nevertheless, we are unable to make another assignment of the sharp lines in the spectra that will lead to a more reasonable number. It is possible that one of the lines observed around 19 847 cm^{-1} is not due to the Ce^{3+} ion, but all of the experimental evidence is consistent with both of the sharp lines assigned in this manner.

It should be noted that three vibronic effects are observed, but are not clearly understood. First, for the first $4f \rightarrow 5d$ transition, there is a significant difference between the one-photon absorption spectrum and the TPE spectrum, with the latter showing much weaker vibronic transitions. In this case, this may be due to the fact that the zero-phonon transition is a fully allowed $4f \rightarrow 5d$ transition including the vibronic transitions. For TPE, however, only the coupling of the $4f$ and $5d$ configurations by the odd components of the crystal field makes this transition observable. This second-order process may result in diminished intensities for the vibronic

TABLE V. Final values of the Hamiltonian fit parameters for the $5d^1$ configuration components of Ce^{3+} in $LuPO_4$. Values in column I were obtained by varying all parameters, values in column II by fixing ζ_{5d^1} at the free-ion value of 995.6 cm^{-1} and varying the remaining parameters.

Parameter (cm^{-1})	I	II
F_0	40 844	40 848
B_0^2	14 846	14 877
B_0^4	17 187	16 694
B_4^4	17 491	17 094
ζ_{5d^1}	9.3	995.6
rms energy deviation (cm^{-1})	4.2	341.0

transitions. Second, for the various TPE lines reported here, there are striking differences between the energies and the relative intensities of the vibronic lines and their associated zero-phonon lines. Finally, the concentration of Ce^{3+} has also been found to play an important role in the vibronic-coupling strength (see Fig. 5). Since the $5d^1$ configuration is not shielded from the crystal environment, as is the $4f^1$ configuration, this effect in itself is expected, but is surprisingly noticeable for small changes in the Ce^{3+} concentration.

In order to understand TPE of Ce^{3+} it is essential to have a systematic study of these vibronic effects. A comparison should be made for Ce^{3+} in different host lattices in a manner similar to that used in the case of single-photon spectroscopic studies of Gd^{3+}.[47]

ACKNOWLEDGMENTS

The work performed at Lawrence Berkeley Laboratory was supported by the Office of Energy Research, Office of Basic Energy Sciences, Chemical Sciences Division of the U.S. Department of Energy under Contract No. DE-AC03-76SF00098. The work performed at Oak Ridge National Laboratory was supported by the Division of Materials Science, U.S. Department of Energy, under Contract No. DE-AC05-84OR21400 with Martin Marietta Energy Systems, Inc. Lawrence Livermore National Laboratory is operated under the auspices of the U.S. Department of Energy under Contract No. W-7405-ENG-48.

* Also at Glenn T. Seaborg Institute for Transactinium Science, Lawrence Livermore National Laboratory, Livermore CA 94550. Electronic mail address: J_SYTSMA@LBL.GOV

[1] J.A. Koningstein and O.S. Mortensen, in *The Raman Effect 2*, edited by A. Anderson (Marcel Dekker, New York, 1973), and references therein.
[2] P.C. Becker *et al.*, Phys. Rev. B **31**, 8102 (1985).
[3] P.C. Becker *et al.*, J. Phys. Chem. **18**, L1066 (1985).
[4] P.C. Becker *et al.*, Phys. Rev. B **45**, 5027 (1992).
[5] G.M. Williams *et al.*, Phys. Rev. B **40**, 4132 (1989).
[6] G.M. Williams *et al.*, Phys. Rev. B **40**, 4143 (1989).
[7] D. Piehler and N.M. Edelstein, Phys. Rev. A **41**, 6406 (1990).
[8] A. Lempicki *et al.*, IEEE Trans. Nucl. Sci. (to be published).
[9] M. Petek, M.M. Abraham, and L.A. Boatner, in *Scientific Basis for Nuclear Waste Management 4* (Elsevier, New York, 1984).
[10] D. Piehler, Ph.D. thesis, University of California at Berkeley, 1990.
[11] L. Smentek-Mielczarek, Phys. Rev. B **46**, 14 453 (1992); **46**, 14 460 (1992); **46**, 14 467 (1992).
[12] W. Kaiser and G.B. Garret, Phys. Rev. Lett. **7**, 229 (1961).
[13] M. Dagenais *et al.*, Phys. Rev. Lett. **46**, 561 (1981).
[14] M.C. Downer, in *Laser Spectroscopy in Solids II*, edited by W.M. Yen (Springer-Verlag, Berlin, 1990).
[15] J.D. Axe, Jr., Phys. Rev. **136**, A42 (1964).
[16] M.C. Downer and A. Bivas, Phys. Rev. B **28**, 3677 (1983).
[17] M.C. Downer, C.D. Cordero-Montalvo, and H. Crosswhite, Phys. Rev. B **28**, 4931 (1983).
[18] B.R. Judd and D.R. Pooler, J. Phys. Chem. **15**, 591 (1982).
[19] C. Cordero-Montalvo and N. Bloembergen, Phys. Rev. B **30**, 438 (1984).
[20] S.K. Gayen and D.S. Hamilton, Phys. Rev. B **28**, 3706 (1983).
[21] S.K. Gayen, D.S. Hamilton, and R.H. Bartram, Phys. Rev. B **34**, 7517 (1986).
[22] R.C. Leavitt, Phys. Rev. B **35**, 9271 (1987).
[23] A.G. Makhanek, V.S. Korolkov, and L.A. Yuguryan, Phys. Status Solidi B **149**, 231 (1988).
[24] S.K. Gayen, Ph.D. thesis, University of Connecticut, 1984.
[25] S.K. Gayen, G.J. Pogatshnik, and D.S. Hamilton, J. Lumin. **31&31**, 260 (1984).
[26] C. Pedrini *et al.*, J. Phys. Condens. Matter **4**, 5461 (1992).
[27] J. Baudry, G.W. Burdick, and J.C. Gacon, Rapport de stage, Université Claude Bernard Lyon-1, 1992 (unpublished).
[28] W.O. Milligan *et al.*, Inorg. Chim. Acta **70**, 133 (1983).
[29] A. Armbruster, R. Thoma, and H. Wehrle, Phys. Status Solidi A **24**, K71 (1974).
[30] *CRC Handbook of Chemistry and Physics*, 70th ed. (CRC, Boca Raton, 1989–1990), p. B-187.
[31] W.O. Milligan *et al.*, Inorg. Chim. Acta **60**, 39 (1982).
[32] T. Hoshina and S. Kuboniwa, J. Phys. Soc. Jpn. **31**, 828 (1971).
[33] E. Nakazawa and S. Shionoya, J. Phys. Soc. Jpn. **36**, 504 (1974).
[34] G. Blasse and A. Bril, J. Chem. Phys. **47**, 5139 (1967).
[35] R.C. Ropp, J. Electrochem. Soc. **115**, 841 (1968).
[36] J.P. Briffault and J.P Denis, Phys. Status Solidi B **41**, 781 (1970).
[37] G. Balasubramian and D.J. Newman, J. Chem. Phys. **36**, 57 (1975).
[38] N.P. Karanjikar and R.C. Naik, Solid State Commun. **65**, 1421 (1988).
[39] T.R. Bader and A. Golf, Phys. Rev. **191**, 997 (1968).
[40] M.M. Denisov and V.P. Makarov, J. Phys. C **5**, 265 (1972).
[41] M. Daoud and M. Kibler (unpublished).
[42] Using the nomenclature of Bader and Gold (Ref. 39), this can be directly verified by taking $(\sqrt{T_\parallel}l, \sqrt{T_\parallel}m, \sqrt{T_\perp}n)$ instead of (l, m, n) as coordinates for the polarization vector.
[43] P.C. Becker, Ph.D. thesis, University of California at Berkeley, 1986. See also Ref. 2, where Raman data are given for the isostructural $ErPO_4$ and $TmPO_4$. Values for $LuPO_4$ are within 4 cm^{-1} of those for $TmPO_4$.
[44] E.N. Yurchenko *et al.*, Izv. Akad. Nauk. SSSR Neorg. Mater. **14**, 2038 (1978).
[45] W.T. Carnall, H. Crosswhite, and H.M. Crosswhite (unpublished).
[46] B. Wybourne, *Spectroscopic Properties of the Rare Earths* (Interscience, New York, 1964), p. 41.
[47] J. Sytsma, W. van Schaik, and G. Blasse, J. Phys. Chem. Solids **52**, 419 (1991).